Curdlan-conjugated PLGA nanoparticles possess macrophage stimulant activity and drug delivery capabilities

Matshawandile Tukulula[1], Rose Hayeshi[1], Pascaline Fonteh[2], Debra Meyer[2#], Abongile Ndamase[1], Michael T. Madziva[3], Vincent Khumalo[1,4], Philip Lubuschagne[1], Brendon Naicker[1], Hulda Swai[1], Admire Dube[1, *]

[1]Encapsulation and Delivery Group, Council for Scientific and Industrial Research, 1 Meiring Naude Road, Brummeria, Pretoria, 0001, South Africa

[2]Department of Biochemistry, Faculty of Natural and Agricultural Sciences, University of Pretoria, Pretoria, 0002, South Africa

[3]School of Physiology, Faculty of Health Sciences, University of the Witwatersrand, 7 York Road, Parktown, Johannesburg, 2193, South Africa

[4]DST/CSIR National Centre for Nanostructured Materials, Council for Scientific and Industrial Research, 1 Meiring Naude Road, Brummeria, Pretoria, 0001, South Africa

Present address: Department of Biochemistry, Faculty of Sciences, University of Johannesburg, P.O Box 524, Auckland Park, Johannesburg, 2006. South Africa

[*]Corresponding author:

Present address: Pharmaceutics Discipline, School of Pharmacy, University of the Western Cape, Bellville, 7535, South Africa

Tel: +27 21 969 2641

Fax: +27 21 959 1324

Email: adube@uwc.ac.za

Suggested running head: **Immunostimulant PLGA nanoparticles**

ABSTRACT

Purpose: There is significant interest in the application of nanoparticles to deliver immunostimulatory signals to cells. We hypothesized that curdlan (immune stimulating polymer) could be conjugated to PLGA and nanoparticles from this copolymer would possess immunostimulatory activity, be non-cytotoxic and function as an effective sustained drug release system.

Methods: Carbodiimide chemistry was employed to conjugate curdlan to PLGA. The conjugate (C-PLGA) was characterized using ^{1}H and ^{13}C NMR, FTIR, DSC and TGA. Nanoparticles were synthesized using an emulsion-solvent evaporation technique. Immunostimulatory activity was characterized in THP-1 derived macrophages. MTT assay and real-time impedance measurements were used to characterize polymer and nanoparticle toxicity and uptake in macrophages. Drug delivery capability was assessed across Caco-2 cells using rifampicin as a model drug.

Results: Spectral characterization confirmed successful synthesis of C-PLGA. C-PLGA nanoparticles enhanced phosphorylated ERK production in macrophages indicating cell stimulation. Nanoparticles provided slow release of rifampicin across Caco-2 cells. Polymers but not nanoparticles altered the adhesion profiles of the macrophages. Impedance measurements suggested Ca^{2+} dependent uptake of nanoparticles by the macrophages.

Conclusions: PLGA nanoparticles with macrophage stimulating and sustained drug delivery capabilities have been prepared. These nanoparticles can be used to stimulate macrophages and concurrently deliver drug in infectious disease therapy.

Key words: immunostimulant nanoparticles, curdlan, PLGA nanoparticles, real-time impedance measurements, rifampicin

ABBREVIATIONS

CI	Cell index
C-PLGA	Curdlan- poly(D,L-lactide-co-glycolide)
DIEA	N,N-Diisopropylethylamine
DSC	Differential scanning calorimetry
DMF	Dimethylformamide
EDC	1-Ethyl-3(3-dimethylaminopropyl)carbodiimide hydrochloride
FTIR	Fourier transform infrared spectroscopy
NMR	Nuclear magnetic resonance spectroscopy
LC-MS	Liquid chromatography mass spectrometry
MTT	3-(4,5-dimethylythiazol-2-yl)-2,5-diphenyltetrazolium bromide
NHS	N-Hydroxysuccinimide
NP	Nanoparticle
PLGA	poly(D,L-lactide-co-glycolide)
PMA	Phorbol myristate acetate
RIF	Rifampicin
ROS/RNS	Reactive oxygen and reactive nitrogen species
SEM	Scanning electron microscope
TEER	Transepithelial electrical resistance
TGA	Thermogravimetric Analysis

INTRODUCTION

In recent times, appreciation of modulation of the immune system to achieve clinically favorable treatment outcomes in diseases has increased. For example, in cancer treatment, much focus is currently placed on 'immuno-oncology', to develop therapies to stimulate cells of the immune system to eradicate cancerous cells [1, 2]. With respect to infectious diseases, a similar approach has been proposed, as a number of infectious disease pathogens typically reside within cells of the immune system in particular, macrophages [3, 4]. In this case, one strategy could be to stimulate the macrophages to self-eradicate intracellular pathogens through action of innate cellular defense mechanisms. This has important implications in treatment of diseases such as tuberculosis (TB) and human immunodeficiency virus (HIV) in which the pathogens may reside in a latent form and these cells serve as infection reservoirs [4]. Pharmaceutical scientists have made significant contributions to the development of polymeric vehicles for delivery of immune-modulatory signals to cells [5]. In a previous study, an immunomodulatory nanoparticle (NP) composed of the immune modulating polysaccharide 1,3-β-glucan adsorbed onto the surface of a chitosan shell, poly($_{D,L}$-lactide-co-glycolide) (PLGA) core NP was described [4]. This NP system could significantly enhance secretion of the pro-inflammatory cytokines IL-12p70, TNF-α and INF-γ and increase generation of reactive oxygen and reactive nitrogen species (ROS/RNS) by alveolar-like macrophages compared to glucan free NPs. 1,3-β-glucans are a family of glucopyranose polysaccharides that consist of 1,3-glycosidic linkages with varying degrees of branching, molecular weight and water solubility [6]. The immune-modulatory properties of β-glucans have been well described [7]. Glucans activate dectin-1, a lectin type cell surface receptor widely expressed by cells of the immune system, in particular, the macrophages. Dectin-1 activation leads to pro-inflammatory gene expression as well as intracellular ROS/RNS production [8].

4

Following the proof of concept of an immune modulating glucan adsorbed NP [4], we hypothesized that curdlan (a linear form of 1,3-β-glucan) could be conjugated to PLGA and NPs from the copolymer would possess macrophage stimulating capability, be non-cytotoxic, and function as a sustained release drug delivery system. Conjugation of curdlan to PLGA would integrate bioactivity into the polymer providing the potential to formulate immune stimulating NPs in a single step. Further, conjugation allows enables easier control of the curdlan density on the NP, through simple variations of molar ratios of curdlan and PLGA during conjugation, or dilution of the copolymer with native PLGA during NP synthesis. Therefore, in this work, we first report a method of conjugating curdlan to PLGA. We then demonstrate stimulation of macrophages by NPs of the copolymerand the sustained drug delivery capability of the NPs *in vitro* and across a model of small intestinal mucosa (Caco-2 cells) using the anti-tubercular drug RIF as a model. Using cell impedance measurements we generate insights into the real-time effects of the polymers and NPs on the macrophages.

MATERIALS AND METHODS

Materials

1-Ethyl-3(3-dimethylaminopropyl)carbodiimide hydrochloride (EDC.HCl), *N*-Hydroxysuccinimide (NHS), *N,N*-Diisopropylethylamine (DIEA), Curdlan from *Alcaligenus faecalis* (molecular weight (MW) 189 kDa), rifampicin (RIF), poly vinyl alcohol (PVA: MW, 13-23 kDa, partially hydrolysed (87-89%)) and poly($_{D,L}$-lactide-*co*-glycolide) (50/50) with the terminal carboxylic acid group (PLGA-COOH: MW, 24-38 kDa) and non-acid terminated (PLGA, MW, 30-60 kDa) were all purchased from Sigma-Aldrich (St Louis, MO). VivaSpin 20 (3000 MWCO polyethersulfone membrane) were purchased from National Separation (Pty) Ltd (Johannesburg, South Africa). All reagents were of analytical grade or above and

were used as purchased unless otherwise stated. Acetonitrile used as mobile phase in high-performance liquid chromatography (HPLC) and liquid mass spectrometer (LC-MS/MS) was purchased from Merck. Deionised water was obtained from a Barnstead EasyPure (II) UV-ultrapure water system (Thermo Fisher Scientific, USA) and was used throughout the study. THP-1 cells were purchased from Highveld Biologicals (Pty) Ltd (Johannesburg, South Africa). Caco-2 cells were obtained from American Type Culture Collection (Rockvillle MD, USA). The media and supplements used to maintain cell growth were purchased from LTC Tech (Johannesburg, South Africa).

Methods

Synthesis of Curdlan-PLGA (C-PLGA) copolymer

The procedure followed for the synthesis of C-PLGA copolymer was adopted from [6, 9], with modification. Curdlan was conjugated to PLGA-COOH as follows: In an oven-dried round bottom flask, Curdlan (50 mg, 0.286 µmoles) was suspended in anhydrous DMF (4 mL) and heated at 60 ºC under N_2 atmosphere until dissolution. In another flask, PLGA-COOH (5.26 µmoles) and NHS (15 µmoles) were stirred in DMF (1 mL) and the mixture cooled to 0 °C in an ice-bath. EDC.HCl (20 µmoles) and DIEA (20 µmoles) were added and the mixture allowed to warm to room temperature and then reacted for 2 h. Upon cooling, the curdlan-DMF solution was added to the 1 mL EDC-activated PLGA solution, and the resultant mixture (curdlan to PLGA ratio 1:20) was further stirred at room temperature for 48 hrs. After this time, the solvent was removed under high *vacuum* to obtain a white amorphous material, which was washed successively with chloroform (10 mL x 5) and water to remove the carbodiimide chemistry byproduct (i.e. urea, which is readily soluble in water [10]). The resulting C-PLGA conjugate was then further washed with de-ionised water (in 3 kDa Vivaspin® tubes at 15000 rpm; 5 minutes each interval), and the product obtained

lyophilised to obtain an amorphous white powder. A schematic of the synthesis of the C-PLGA is shown in Figure 1. For synthesis of copolymer for use in NP synthesis, the curdlan-PLGA solution obtained in the steps above was diluted with non-acid terminated PLGA (50:50; Mw 30 – 60 kDa) and stirred for another 24 h to obtain an overall 1% curdlan loading in the mixture after lyophilization. Dilution to 1% curdlan was performed to mitigate the poor solubility of C-PLGA in the organic solvents used in NP synthesis and also to avoid any potential detrimental over stimulation of the macrophages by high concentrations of curdlan.
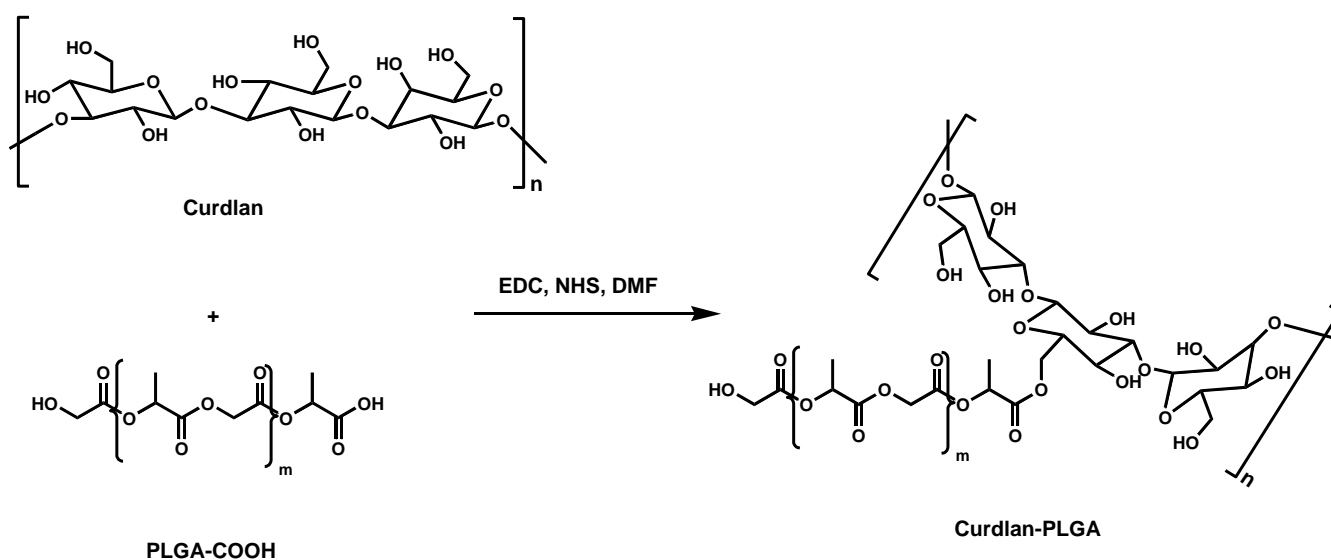
Figure 1: Schematic of synthesis of C-PLGA copolymer. Acid terminated PLGA is reacted with curdlan to produce C-PLGA conjugate (*Reagents and conditions*: *EDC*.HCl, *NHS*, *DIEA*, DMF, rt, 48 h).

Characterization of polymers

Polymers (PLGA, C-PLGA and curdlan) were characterized by ^{1}H and ^{13}C NMR (Bruker 400 MHz Avance III HD Nanobay instrument using a 5mm BBO probe on Topspin 3.2) using tetramethylsilane as an internal standard and DMSO-d_6 as the solvent, and by FTIR (Perkin Elmer: Spectrum 100, in attenuated total reflectance mode from 550 to 4000 cm^{-1}). Thermal behavior was characterized by TGA in a Q500 device (TA instruments TGA 2960) in ramp mode from room temperature to 700 ºC at the rate of 10 ºC/minute under nitrogen)

and by DSC (Perkin Elmer DSC Q2000) in the temperature range of 20 to 150 °C using the ramp method at the rate of 10 °C/minute under nitrogen atmosphere. DSC sample analysis was accomplished by weighing 4-10 mg of the material and sealing it in an aluminum sample pan, and an empty pan was used as a reference. Samples were run in triplicate.

NP preparation and characterization

C-PLGA NPs were synthesized using an emulsion solvent evaporation technique adopted with modifications from reference [4]. 20 mg/mL C-PLGA copolymer solution in DMF: chloroform (20:80) was added drop-wise to 10 mg/mL PVA solution in de-ionised water, under stirring at 1000 rpm. Upon complete addition, the suspension on ice was subjected to high speed homogenization at 8000 rpm for 10 minutes using a Silverson L4R mixer homogenizer (Silverson, MA). Organic solvents were subsequently removed *in vacuo* and the NPs collected through centrifugation at 15 000 rpm for 5 min, followed by washing three times with de-ionized water and lyophilized over a period of 72 h in the presence of 1% sucrose as a cryoprotectant. PLGA NPs were also synthesized using an emulsion-solvent evaporation technique. However, in this instance a 20 mg/mL PLGA solution was prepared in ethyl acetate. To synthesize RIF loaded NPs, the procedure as described above was followed, except that the ethyl acetate or DMF/chloroform mixture contained 2 mg/mL RIF.

The particle size, polydispersity index and zeta potential were measured using photon correlation spectroscopy techniques using a Malvern Zetasizer NanoZS (Malvern Instruments, UK) with measurements conducted at 25 °C and at an angle of 173°. Approximately 1 mg of the NP was suspended in 1 mL de-ionised water with vortexing and sonication. The intensity-weighted mean value was determined and the average of three measurements taken. Scanning electron microscopy (SEM, Phillips XL 30, scanning

microscope, Phillips, Eindhoven, The Netherlands) was used to determine the shape and surface morphology of the NPs produced. Particles were coated with carbon under vacuum before SEM.

Characterization of drug loading and in vitro drug release

The amount of RIF loaded in the NPs (µg RIF per mg NP) was determined as described previously [4]. Briefly, 1 mg NPs was sonicated in 600 µL acetonitrile for up to 5 min to breakup the NPs. To the suspension in acetonitrile, 400 µL of 10 mM phosphate buffer pH 6.6 was added (to match the HPLC mobile phase). This suspension was centrifuged at 15 000 rpm for 5 min, before 50 µL of the supernatant was injected onto an HPLC/UV system for quantitation of RIF (assay conditions described below). To characterize drug release, RIF loaded NPs (1 mg/mL) were incubated in phosphate buffer pH 7.4 containing 5 mg of ascorbic acid per 10 mg of NP (to mitigate oxidative degradation of RIF) at 37 °C in a shaking water bath (100 rpm) over 6 h. At set time points, the NPs were removed from the bath, centrifuged at 15 000 rpm for 5 min, and the supernatant collected and analysed for RIF concentration using a validated HPLC method (described below). Samples were diluted with acetonitrile before injection, in order to match the HPLC mobile phase.

Transportation of RIF across a Caco-2 cell monolayer

As the oral route is common for administration of anti-infectives, the capability of the NPs to deliver RIF across intestinal tissue was assessed using a Caco-2 cell model. Caco-2 cells were cultured in medium consisting of Dulbecco's Modified Eagle Medium (DMEM), high glucose with glutamine, foetal bovine serum, penicillin and streptomycin. The cells were maintained in culture flasks in an incubator with the following conditions; 5% CO_2 atmosphere, 37 °C, 90 % relative humidity. Cells were passaged upon reaching 80-90 %

confluence and were seeded on 30 mm polycarbonate membranes with a pore size of 0.4 μM and an area of 4.2 cm^2 (Millicel, Millipore, USA) at a concentration of 10 000 cells/cm^2 and maintained at 37 °C in a humidified atmosphere with 5 % CO_2. Cells were ready for use 21 days post-seeding. Apical to basolateral transport studies were performed as previously described [11] with slight modifications. The buffer used was HBSS buffered with 25 mM HEPES at pH 7.4. Caco-2 cells, 21 days post seeding, were equilibrated in pre-warmed HBSS for 15 min at 37 °C and the trans-epithelial electrical resistance (TEER) measured. 1 mL HBSS was added to the apical compartment and 2 mL to the basolateral compartment. 100 μL of the preparations (approximately 1 mg/mL NPs suspended in water containing 1 μg/mL RIF; or 1 μg/mL RIF in water) was then spiked into the apical compartment. The plates were incubated at 37 °C in a shaking incubator at 450 rpm, to minimize the unstirred water layer. At the beginning and end of the experiment an aliquot was withdrawn from the apical solution (the donor) to determine initial and final donor concentrations. At selected time intervals from 0 to 6 h, an aliquot was withdrawn from the basolateral side, and replaced with fresh HBSS. At the end of the experiment TEER was measured to determine whether the test preparations had any effect on the integrity of the cells. Samples collected were spun down (10 000 rpm for 10 min) to remove cellular debris and/or NPs, and the supernatant collected for assay of RIF using a validated LC-MS assay (described below). The concentration of RIF measured over time was converted into flux (μg/cm^2/h) representing the rate of translocation of the drug across the tissue.

HPLC and LC-MS assay

The HPLC/UV system comprised of Shimadzu Prominence HPLC series (Shimadzu Corporation, Kyoto, Japan) with a CBM-20A controller bus module, LC-20AT liquid chromatograph, CTO-10AS VP column oven and SPD Diode array detector. RIF was eluted

under isocratic conditions using 60:40 v/v 10 mM phosphate buffer pH 6.6: acetonitrile, at a flow rate 1 mL/min and detection wavelength 254 nm. A calibration curve of RIF mass on column versus absorbance with linearity over the range 0.0025 to 0.02 µg ($r^2 \geq 0.99$) was used to quantify the RIF extracted from the NPs and in the drug release study.

The LC–MS/MS system consisted of a Shimadzu Prominence Ultra-Fast LC (UFLC) series system (Shimadzu Corporation, Kyoto, Japan) coupled with an ABSciex 3200 QTrap Triple Quadrupole Tandem Mass Spectrometer equipped with Analyst 1.6 software (AB Sciex, Massachusetts, USA). Chromatography was performed using a 9 min gradient elution method with 0.1% formic acid (FA) as mobile phase A and acetonitrile (0.1% FA) as mobile phase B at a flow rate of 0.5 mL/min on a Phenomenex Kinetex 2.6 µ C8 analytical column (50 mm x 4.60 mm). Briefly, the time program for the gradient method used was: 2% B for 1 min; ramped up to 98% B until 2 min; held at 98% B until 7 min; ramped down to 2 % B until 8 min; equilibrated at 2% B until 9 min. The mass spectrometer was operated in positive ion mode with the transition of 823.4 m/z –791.4 m/z for RIF detection. The following ion source parameters were used: curtain gas flow, 35 psi; ion spray voltage, 4500 V; temperature, 500 °C; gases 1 and2, 45 psi; declustering potential, 45 V; entrance potential, 4V; collision cell entrance potential, 28.87 V; collision energy, 25 V and collision cell exit potential, 6.1 V. The parameters for the quantification method: peak areas integrated; expected retention time of RIF, 3.04 min; 30 sec RT window; noise percentage, 50%; peak splitting factor, 2; smoothing width, 5 points; linear fit calibration curve; no weighting of calibration points. The range of the assay was 5 ng/mL to 1 µg/mL ($r^2 \geq 0.99$).

Determination of macrophage stimulatory capability of the NPs: phosphorylated ERK production in THP-1 derived macrophages

THP-1 cells were routinely maintained at 37°C in a 5% CO_2 humidified incubator. The growth medium used was RPMI-1640 medium with GlutaMAX (Gibco), supplemented with penicillin (50 µg/mL), streptomycin (50 µg/mL) and 10% heat inactivated foetal calf serum. THP-1 cells (1×10^6 cells per well) were plated into a 6-well plate in growth medium containing phorbol-12-myristate-13-acetate (PMA, 50 nM) for 48 h. PMA differentiates THP-1 cells into macrophage-like cells. PMA free growth medium was added for an additional 24 h. In duplicate wells, 100 µL (of 1 mg/mL NP suspension in water) of PLGA NPs or C-PLGA NPs was added to the cells. Curdlan (100 µL of 1 mg/mL aqueous solution) was used as a positive control. The NPs used were not loaded with RIF to avoid any confounding effects arising from the drug. After 5 min of incubation at 37°C, the cells were washed with ice-cold PBS to remove the particles, and were immediately lysed by incubation in lysis buffer (50 mM Tris·HCl pH 7.4, 150 mM NaCl, 0.5% EDTA, 1% Triton-X 100, 0.1% sodium dodecyl sulphate (SDS), 50 mM NaF, 30 mM $Na_4P_2O_7$ and 100 µM Na_3VO_4 containing the Complete™ (Roche) protease inhibitor cocktail). Cell lysates were centrifuged (12 000 rpm, 15 min) and supernatants were mixed with an equal volume of 2X sample buffer (100 mM Tris HCl pH 6.8, 10% glycerol, 4% SDS, 0.01% bromophenol blue and 200 mM β-mercaptoethanol) and incubated for 20 min. Proteins were separated by SDS polyacrylamide gel electrophoresis and transferred to nitrocellulose (BioRad, Johannesburg, South Africa) using a blotter (BioRad). The nitrocellulose was blocked for 1 h in blocking solution (20 mM Tris·HCl pH 7.5, 150 mM NaCl, 5% powdered milk, 0.1% Tween-20) and phosphorylated ERK was detected using a polyclonal rabbit anti-phospho-ERK antibody (1:1000, Cell Signaling, Danvers, MA) overnight at 4°C. The blot was washed (three times over a period of 10 min, blocking solution) and incubated with horseradish

peroxidase-coupled anti-rabbit secondary antibody (1:1000, Cell Signaling 1 h, room temperature). After three more 10 min washes in blocking solution, the proteins were visualized by enhanced chemiluminesce (BioRad).

Characterization of cell viability, adhesion, proliferation and morphology in the presence of polymers and NPs

The 3-(4,5-dimethylythiazol-2-yl)-2,5-diphenyltetrazolium bromide (MTT) assay and the impedance technology of the real time cell electronic sensing analyzer (RT-CES™, ACEA Biosciences Inc., San Diego, USA) were used for determining cytotoxicity on the THP-1 derived macrophages. For both assays, a pre-determined cell density of 40,000 cells/well was used and THP-1 cell differentiation performed as described above.

The MTT assay quantifies mitochondrial dehydrogenase activity as a measure of cell viability [12]. Polymer and NP concentrations in the range 0.13-200 µg/mL were tested, and viability was determined at 24 h and 72 h post treatment as per method previously described [13]. Polymer solutions and NP suspensions were prepared in water. However, polymer solutions were initially dissolved in DMSO to aid solubility (final concentration in culture ≤1%). We established that this concentration of DMSO did not affect the viability of the cells as demonstrated by control cells. The concentration of the polymers or NPs that produced 50% of cell growth inhibition (IC_{50}) was estimated from plots of cell viability (%) versus concentrations (µg/mL).

RT-CES™ provides an indirect measurement of viability [14-16] and cytotoxicity [17] by measuring the impedance or cell index (CI) produced as cells attach on the surface of an electronic (E)-plate. The background of the E-plates was determined for 1 min in 100 µL of complete RPMI and this was subsequently replaced with 200 µL of 40 000 THP-1 cell

suspension containing 50 nM PMA. After equilibrating the E-plates at room temperature for 30 min THP-1 differentiation and adhesion profile was automatically monitored for 48 h (with 50 nM PMA) and for an additional 24 h (PMA-free) before treatment with 0.4, 40 or 100 µg/mL of PLGA and C-PLGA polymers or NPs (PLGA NP, C-PLGA NP). Polymer solutions contained ≤1% of DMSO to aid solubility. The profile of the treated cells was further monitored for an additional 72 h. At the start of each adhesion phase, impedance was measured short term every 1 min and subsequently every 30 min to determine both transient and long term effects respectively. Increases in CI relative to untreated controls were interpreted as cell viability (adhesion), cell spreading (swelling) or cell proliferation, while decreases were associated with cytotoxicity or cell detachment resulting from changes in adhesion properties. Microscopic examination of the cells was performed using an inverted microscope (Zeiss Axiovert 40 C, Carl Zeiss Inc., Thornwood, NY) to assess any morphological changes.

Statistical analysis

Data were analyzed for statistical differences by the Students' t-test using the Statistical Package for Social Science v 22 (IBM, SPSS, Chicago). Statistical differences were considered at $p < 0.05$. All data are presented as mean ± s.d., unless otherwise stated.

RESULTS AND DISCUSSION

Synthesis and characterization of C-PLGA

Synthesis of the C-PLGA copolymer was carried out as shown in Figure 1 and verified by NMR, FTIR, TGA and DSC. The NMR fingerprint of pure PLGA and curdlan correlated with literature [18, 19]. The ^{1}H NMR spectrum of C-PLGA (Figure 2) reveals a new peak at 3.69

ppm which is attributed to the presence of curdlan's OCH_2 groups in the copolymer. Similarly, the ^{13}C NMR spectrum of C-PLGA (Figure 3) revealed peaks resonating at 87.7
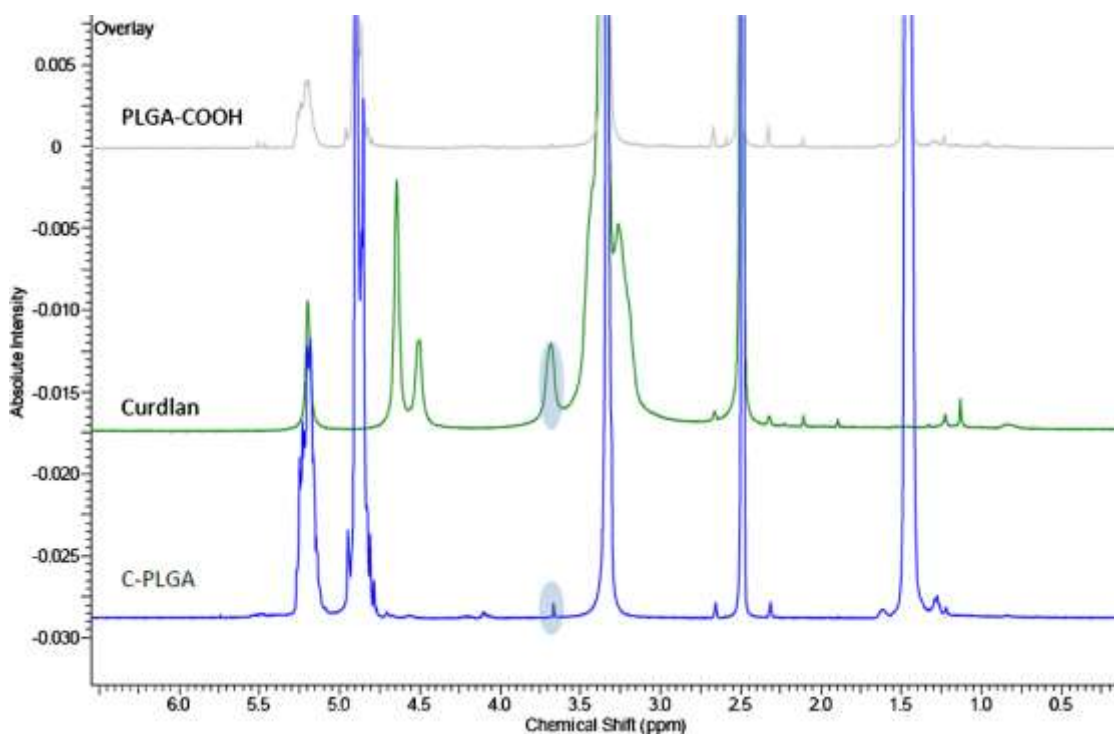

Figure 2: ^1H NMR spectra of PLGA-COOH, curdlan and C-PLGA copolymer. C-PLGA spectra reveals new peak (highlighted) at 3.69 ppm attributed to the presence of curdlan OCH_2 groups.
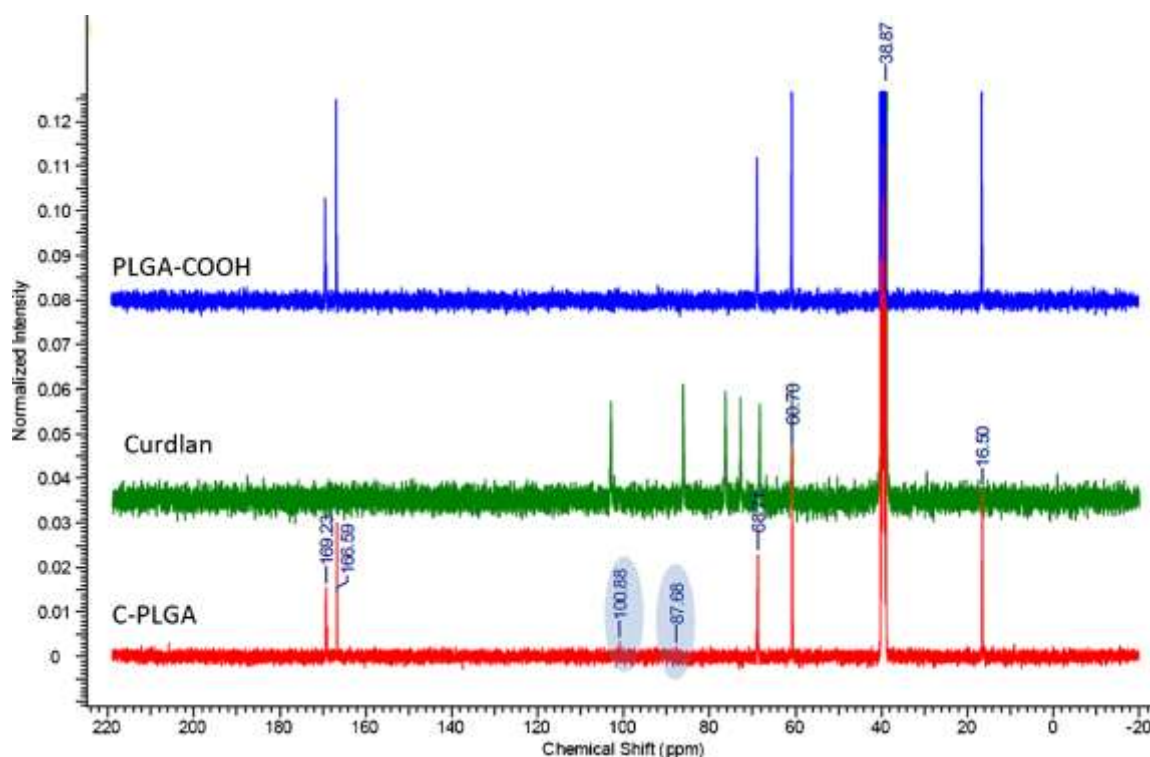

Figure 3: ^{13}C NMR spectra of PLGA-COOH, curdlan and C-PLGA copolymer. C-PLGA spectra reveals new peaks resonating at 87.7 and 100.9 ppm, attributed to the carbons of the curdlan backbone in the copolymer.
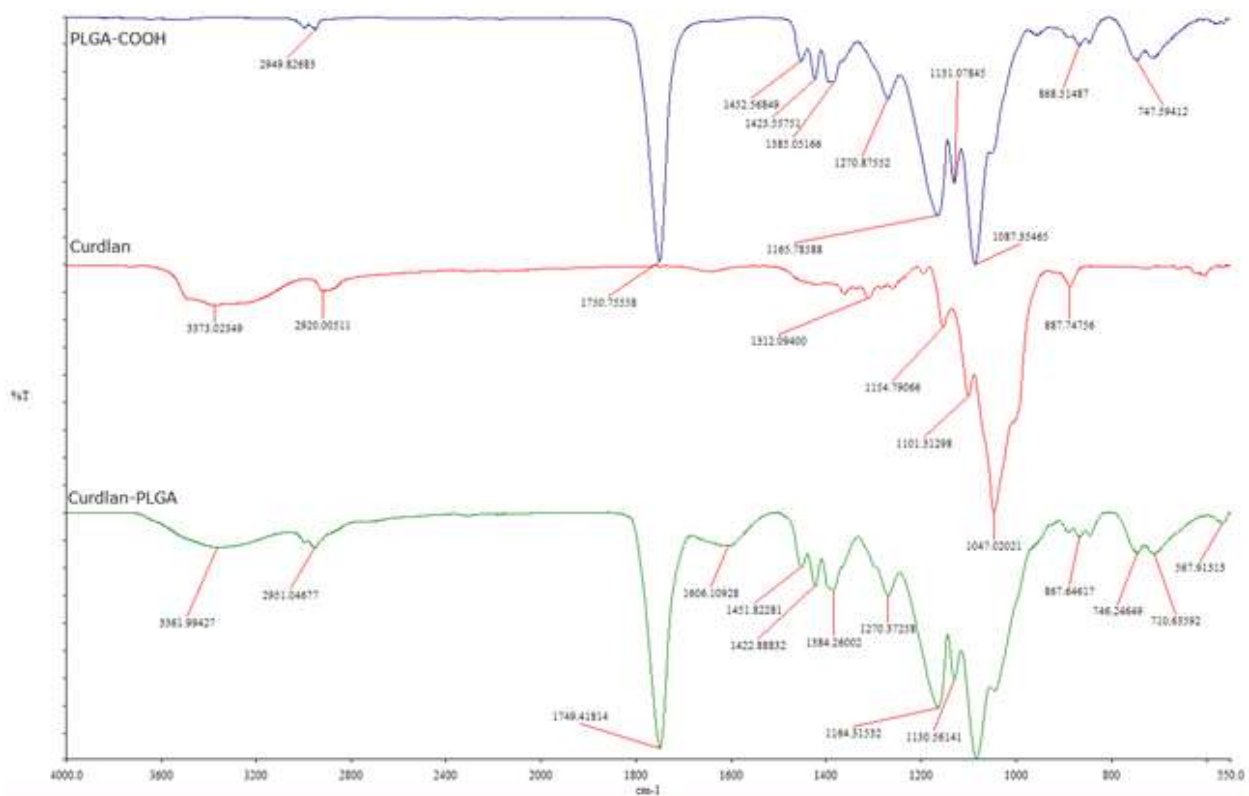
Figure 4: FT-IR spectra of acid terminated PLGA-COOH, curdlan and Curdlan-PLGA copolymer.

and 100.9 ppm, also attributed to the carbons of the curdlan backbone in the copolymer. The percentage amount of curdlan grafted onto the PLGA-COOH backbone was found to be about 3%, calculated from the intensity of the peak resonating at 3.69 ppm vs that of PLGA-COOH resonating at 5.62 ppm in the ^{1}H NMR, and peaks at 100.9 ppm vs that of PLGA-COOH at 68.7 ppm in the ^{13}C NMR. The FTIR spectrum (Figure 4) of PLGA-COOH exhibited strong characteristic adsorption peaks/bands at about 1750.8, 1452, 1180-1129 cm^{-1} which correspond to the C-O (carbonyl), C-O-C (ether) and C-H (methyl) bonds, respectively. Furthermore, for pure curdlan the strong band at 3373.0 cm^{-1} corresponds to OH (hydroxide) bond, while those in the region 2920.0, 1100-1190 and 892.5 cm^{-1} corresponds to the CH stretching, C-O-C bonds and the β-linked glycosidic bridges found in polysaccharides, respectively. In the case of the C-PLGA conjugate, all the characteristics of the pure PLGA and curdlan were pronounced, thus indicating the successful formation of the conjugate.

16

Figure 5 shows the TGA curves over the temperature range 25 – 700°C of PLGA-COOH, curdlan and C-PLGA. Curdlan shows two stages of weight loss, firstly a gradual weight loss of ±4.5wt% between 25°C and 250°C, which can be attributed to the desorption of \
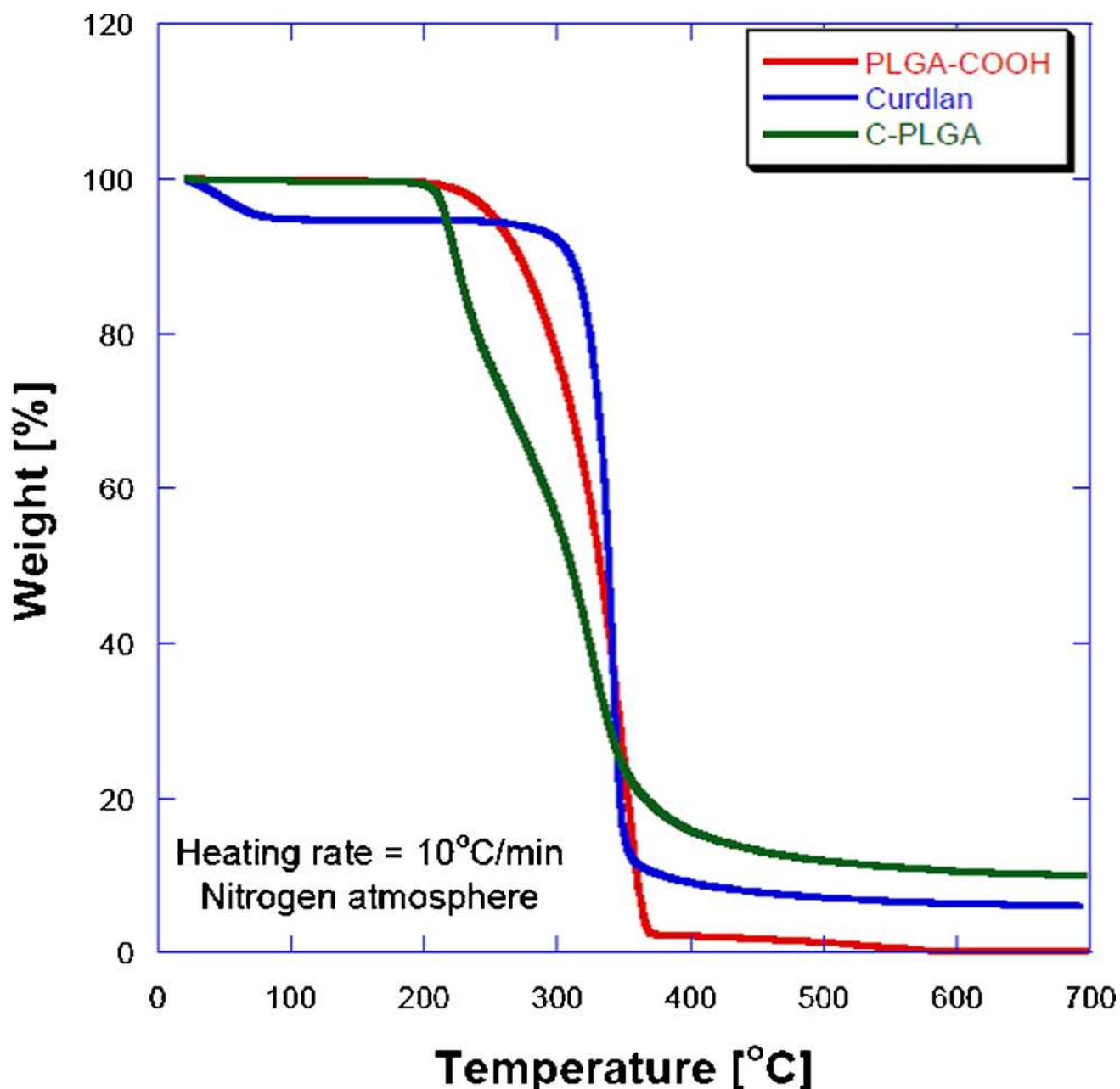

Figure 5: TGA thermogram curves of PLGA-COOH, curdlan and Curdlan-PLGA.

adsorbed and bound water [20], and secondly from 250 – 380°C which is attributed to curdlan decomposition. Both PLGA-COOH and C-PLGA shows a single weight loss stage attributed to thermal decomposition. The onset temperatures of decomposition for both PLGA-COOH and C-PLGA is ±200°C, with C-PLGA showing a faster decomposition rate

with 23.6wt% loss at 250°C, while at the same temperature PLGA-COOH shows 4.5wt% loss. Previous studies have shown that the grafting of molecules onto a polymer chain can reduce thermal stability due to the incorporation of some "weak links" into the polymer structure [21, 22]. A further indication of conjugation can be obtained from changes in the char residue, as previous studies have shown that greater residues are associated with increased grafting yields [22, 23]. PLGA-COOH and curdlan show char residues of 0.3 and 5wt%, respectively, while C-PLGA shows a residue of 10 wt%.

DSC analysis of PLGA-COOH, curdlan and C-PLGA were conducted as shown in Figure 6. Two heating scans were performed as the first heating is affected by thermal history of the polymer, and therefore does not reliably indicate the original polymeric properties. No
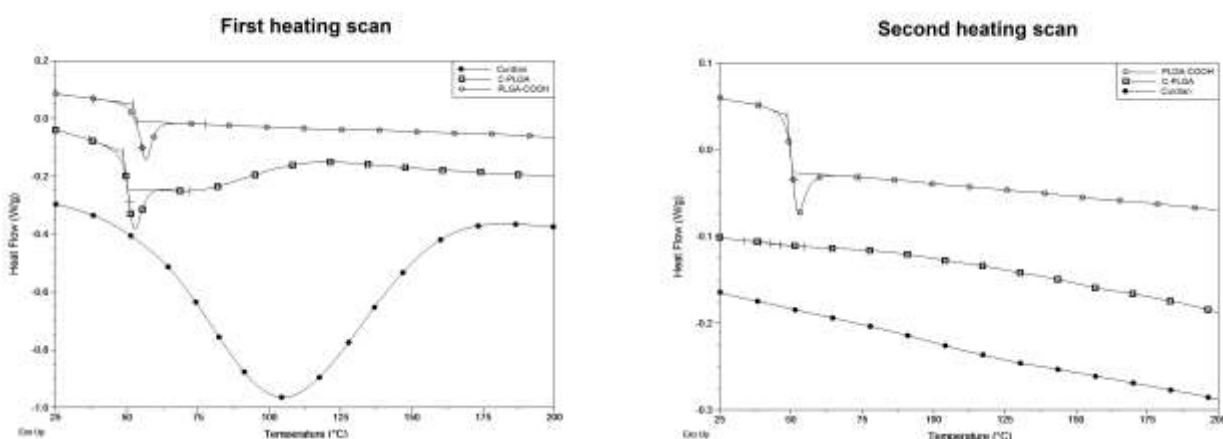

Figure 6: DSC curves (1st and 2nd melt) for PLGA-COOH, curdlan and Curdlan-PLGA.

thermal events were detected in the cooling scan (data not shown). In the second scan PLGA-COOH shows a glass transition temperature (T_g) of 50.6 ± 0.2°C, while the C-PLGA conjugate shows a more subtle T_g of 42.5 ± 0.2°C. No thermal transitions are shown for curdlan in the same temperature range, with only a broad symmetric endotherm of water thermodesorption at 100.5 ± 6.7°C in the first heating scan. The slight decrease in T_g of the C-PLGA sample would suggest PLGA-COOH microphase separation induced by the presence of curdlan. This phenomenon is known to occur after grafting or conjugation

reactions onto polymers [24-26]. Additionally, the presence of molecules bound to a polymer could favour unobtrusive motion of the polymer chains due to increased free volume, which could be reflected by a subtle T_g [27]. Taken together our characterizations confirm the successful formation of the C-PLGA copolymer.

Table 1: Characteristics of the PLGA and C-PLGA nanoparticles (empty and drug loaded).

Samples	Size (nm)	PDI	Zeta potential (mV)	Drug loading (µg/mg)
PLGA	286.9 ± 9.9	0.23 ± 0.03	-16.5 ± 0.1	-
PLGA(RIF)	264.3 ± 4.6	0.12 ± 0.04	-11.6 ± 0.5	1.16 ± 0.05
C-PLGA	486.8 ± 26.6	0.42 ± 0.01	-25.9 ± 0.3	-
C-PLGA(RIF)	301.2 ± 5.5	0.19 ± 0.03	-29.9 ± 0.1	1.05 ± 0.03

Characterization of the PLGA and C-PLGA NPs

The physicochemical characteristics of the PLGA and C-PLGA NPs are presented in Table 1. The C-PLGA NPs had significantly greater ($p < 0.05$) size and zeta potential compared to the PLGA NPs. This was also the case for the RIF loaded C-PLGA NPs. This was expected given the incorporation of curdlan onto the PLGA backbone. It is possible that the use of different organic solvents, i.e. ethyl acetate in the case of PLGA NPs and DMF/chloroform in the case of C-PLGA NPs, could have resulted in the differences in particle size observed. However, studies which have evaluated the impact of variations in organic solvents on PLGA particle size, indicate that NP size changes occurring due to differences in organic solvents are relatively small [28], and therefore we deduce that the size changes observed in this study are due to the presence of curdlan. SEM analysis of the NPs (Figure 7) revealed that spherical NPs were formed from both polymers. No differences in surface characteristics could be observed between the PLGA and the C-PLGA NPs. SEM of the

19

RIF loaded NPs showed images similar to the drug-free NPs (data not shown). Approximately 1 µg of RIF could be loaded per mg of NPs which was acceptable to characterize the performance of the NPs with respect to drug release and intestinal transport.
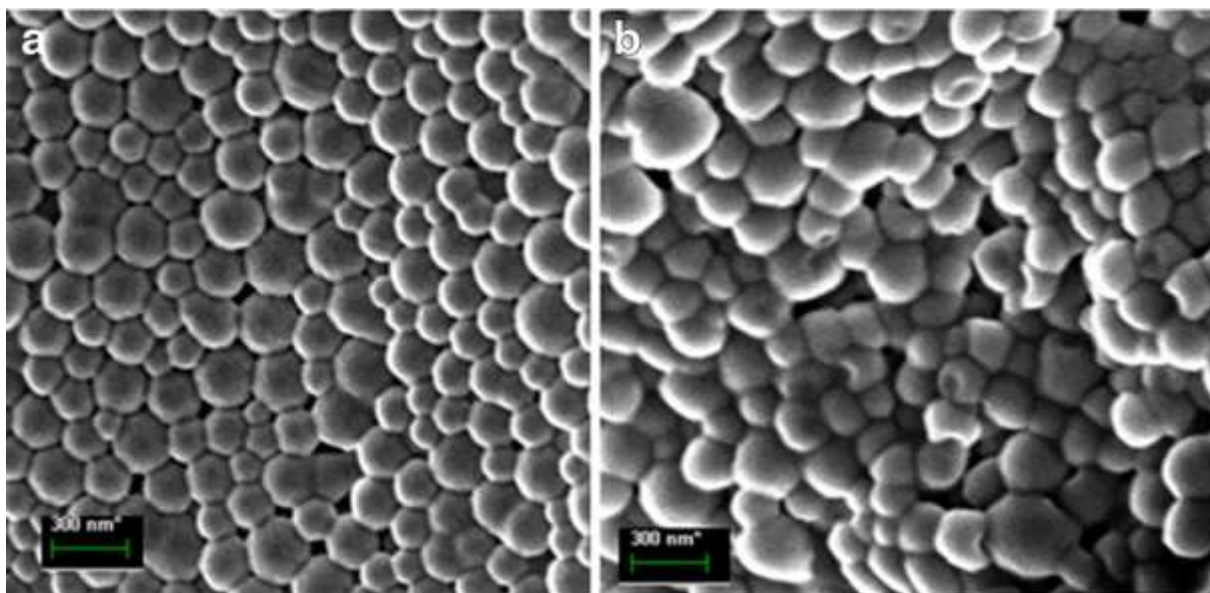

figure 7. Fig. 7 Scanning electron micrographs of (a) PLGA NPs and (b) C-PLGA NPs.
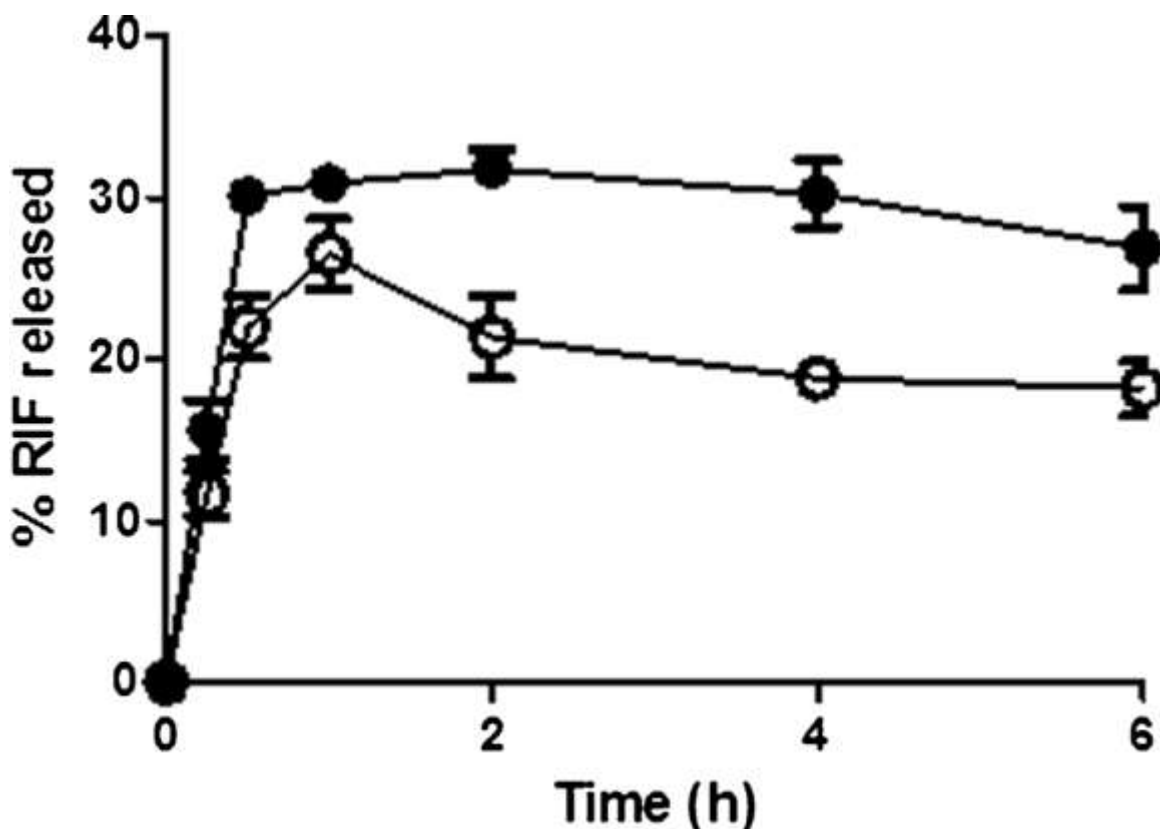

Figure 8: Cumulative in vitro release profiles of RIF from the PLGA (-●-) and CPLGA (-○-) NPs in phosphate buffer pH 7.4 at 37°C over a 6 h period.

In-vitro drug release profiles

A characteristic biphasic release profile was observed (Figure 8) i.e. an initial burst phase (occurring up to 1 h, and representing release of up to 30% of drug cargo), followed by a sustained release phase. Drug release was tracked up to 6 h and at this time point $26.9 \pm 2.6\%$ and $18.2 \pm 1.2\%$ of encapsulated RIF had been released by the PLGA NPs and C-PLGA NPs, respectively. This suggested that the majority of the encapsulated drug was still present within the core of the NPs and needed a longer period for complete release. We attempted to track drug release at 24 h and beyond (data not shown), however we observed a trend of decreasing drug concentrations indicating the reduced protection of RIF by ascorbic acid at time points beyond 6 h. Therefore data beyond 6 h could not be used to describe the drug release performance of the NPs. The C-PLGA NPs released significantly less drug ($p < 0.05$) than the PLGA NPs at both 1 h and 6 h, suggesting that incorporation of curdlan enhanced the sustained release properties of PLGA NPs. It would not be unreasonable to assume that the copolymer make-up of the C-PLGA NPs could retard rates of drug diffusion and/or have reduced rates of polymer erosion in comparison to PLGA NPs. The sustained drug release profiles observed under these pH conditions suggests the potential of the NPs to provide sustained plasma, trans-intestinal and intracellular (cytoplasm) drug concentrations.

RIF flux across Caco-2 cell monolayer

The flux ($\mu g/cm^2/h$) of RIF across an intestinal monolayer (Caco-2 cells) was assessed. We observed that RIF had a significantly greater flux ($p < 0.05$) across the intestinal model of Caco-2 cells as a free solution than when encapsulated in the NPs (Figure 9). RIF flux (as solution) was 2.3 and 3.1 fold greater than when it was delivered by the PLGA NPs and C-PLGA NPs, respectively. There was no significant difference ($p > 0.05$) in RIF flux between
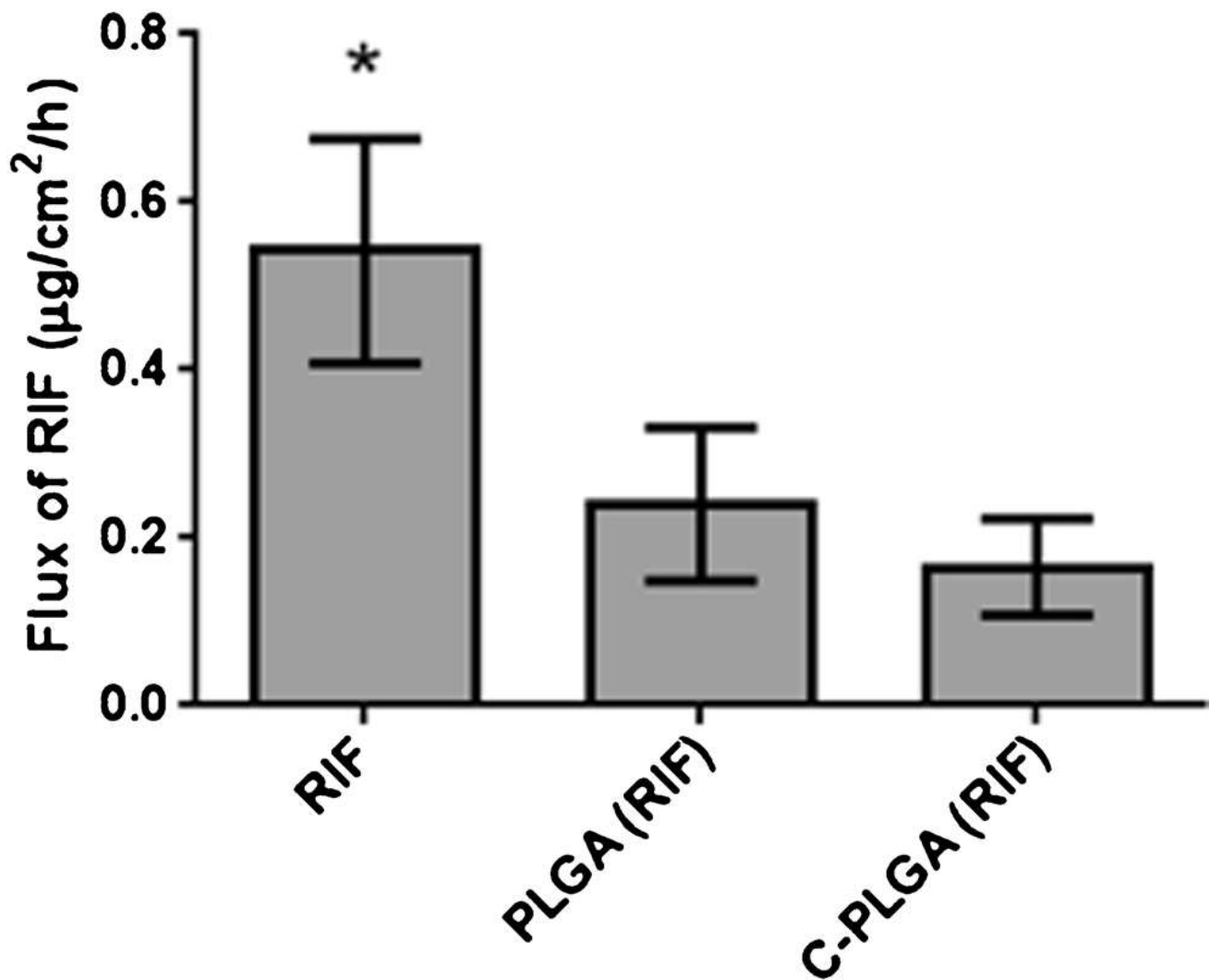
Figure 9: Rate of translocation of rifampicin (RIF), expressed as flux (μg/cm2/h) across caco-2 cells as drug solution (RIF) and delivered by NPs (PLGA (RIF) and C-PLGA (RIF). * A statistically significant difference ($p < 0.05$) was observed in the flux of RIF as a solution compared to NPs.

the PLGA NPs and C-PLGA NPs over 6 h. The driving force for flux is the concentration gradient of 'free' drug (i.e. drug not encapsulated in NPs) across the donor and receptor sides of the membrane. As encapsulated RIF was released slowly, and remained predominantly encapsulated, flux would be expected to be slower for the NP encapsulated RIF compared to RIF solution. Therefore, the reduced flux suggests that the NPs could serve as a system for sustained RIF delivery across the intestine. Sustained drug concentrations would be beneficial for continued killing of microbes and preventing generation of drug resistant strains, provided the delivered concentrations are continually

above the minimum inhibitory concentrations. However, further studies in animals to characterize plasma and tissue concentrations of drug delivered by the NPs are warranted.

Stimulation of phosphorylated ERK production in macrophages

Macrophages were stimulated in duplicate with either 100 µg/mL of PLGA NP, C-PLGA NP or curdlan (positive control), and cells assayed for phosphorylated ERK production. Phosphorylated ERK is an upstream mediator of ROS/RNS and is therefore indicative of immune-stimulation [29]. Figure 10 shows phosphorylated ERK generated after 5 min of
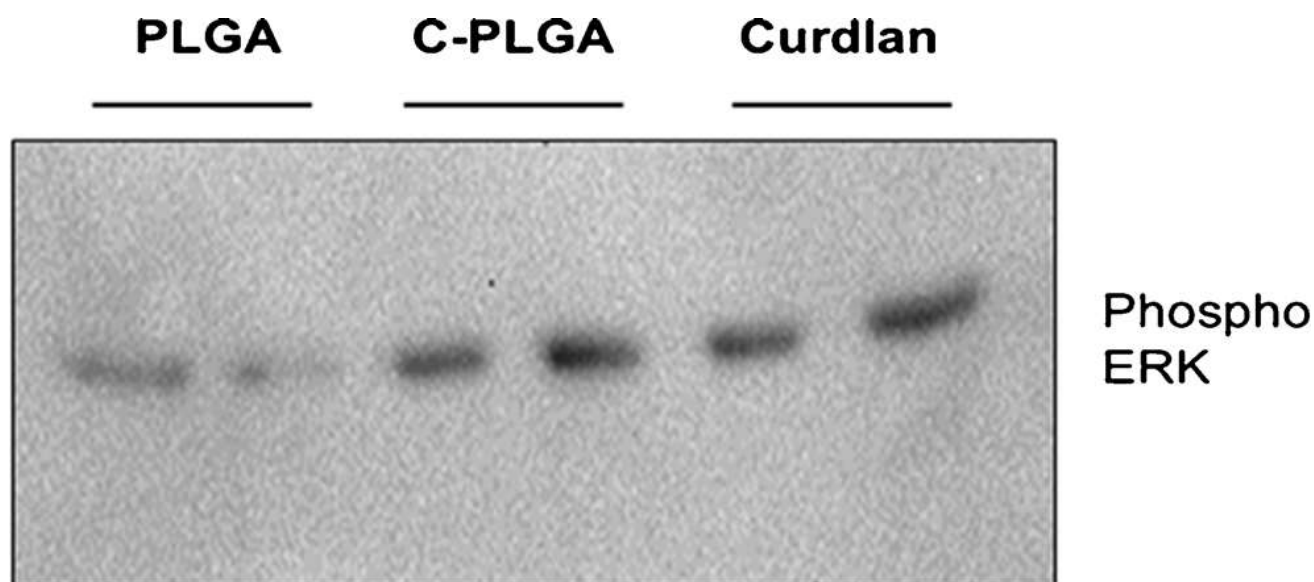

Figure 10: Phosphorylation of ERK in THP-1 derived macrophages. Macrophages were stimulated in duplicate with PLGA NPs, C-PLGA NPs and curdlan as described under Materials and Methods. The cells were lysedand phosphorylated (phospho) ERK was detected by western blotting. This gel is a representative gel of two separate experiments.

stimulation. Basal production of phosphorylated ERK in the cells stimulated with PLGA NPs was observed. Stimulation of the cells with C-PLGA NPs resulted in enhanced production of phosphorylated ERK. This activation of ERK by C-PLGA NPs was similar to that of curdlan-only treated cells and supports the hypothesis that NPs from the C-PLGA would possess immune-stimulatory activity. These results are also in line with previous observations of enhanced stimulation of alveolar-like macrophages by 1,3-β-glucan adsorbed chitosan-PLGA NPs in comparison to chitosan-PLGA NPs [4]. We believe cellular stimulation could

23

be an important adjunct approach (together with drug action) in the eradication of intracellular pathogens, particularly in the case of pathogens such as *M.tb* which are able to switch off the antimicrobial response of the macrophage, and remain dormant within these cells for long periods of time [30]. Our data suggests enhanced macrophage production of ROS/RNS which is known to be toxic to intracellular pathogens and trigger cytocidal reactions as part of the host pathogen defense strategy [31].However, studies in pathogen infected macrophages are warranted to prove efficacy of this approach..
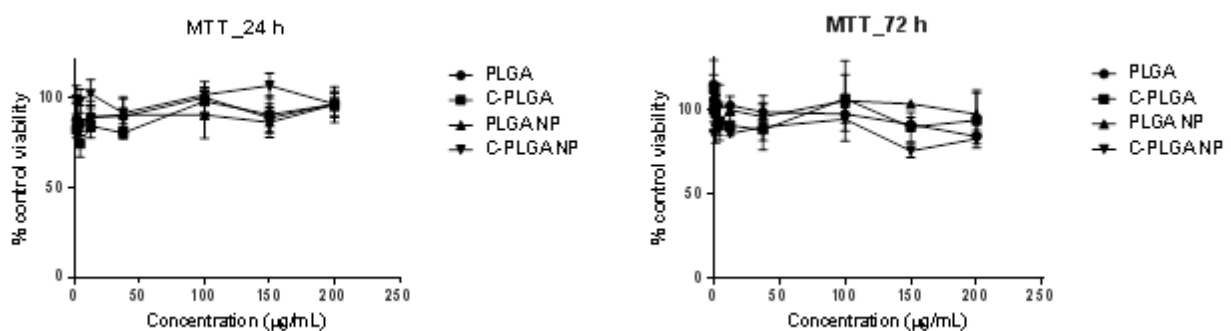

Figure 11: The effect of the polymers and nanoparticles on the viability of THP-1 derived macrophages. At concentrations ranging from 0.13 to 200 μg/mL, the polymers and polymer nanoparticles did not affect cell viability. The results are means of 4 independent repeats and the error bars represent SEM..

Cell viability, proliferation, adhesion and morphological changes in the presence of polymers and NPs

The target site of action of the NPs is the macrophage, therefore it was important to characterize any toxicity of the polymers and NPs on the macrophages. The effect of the polymers and NPs on the viability of THP-1 derived macrophages was assessed using the MTT assay. Polymers (PLGA and C-PLGA) as well as the PLGA NPs and C-PLGA NPs did not adversely affect the viability of the macrophages over a 72 h period (Figure 11). The IC_{50} for all treatments was found to be >200 μg/mL suggesting that the polymers and NPs were not toxic.
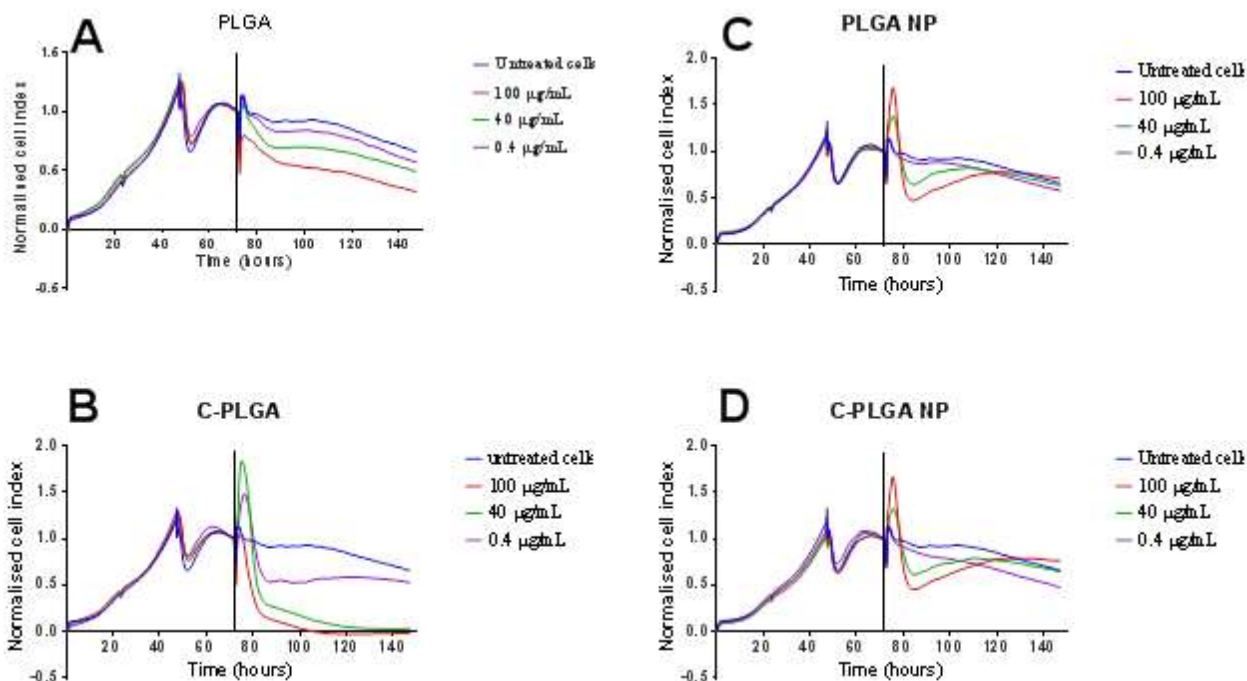
Figure 12: Effect of PLGA, C-PLGA, PLGA NPs and C-PLGA NPs on the proliferation profile of THP-1 derived macrophages monitored by RT-CES™ analyser. Dose response patterns were observed depicting uptake of C-PLGA, PLGA NPs and C-PLGA NPs and "spoon shaped" profiles for PLGA NPs and C-PLGA NPs in a concentration dependent manner. The uptake response was reversed with respect to dose for the polymers compared to the NPs likely due to dose dependent effects of the polymers on cell adhesion. Loss of cell adhesion results in reduced CI. The data was represented as normalized CI (vertical line at 72 h) to account for differences in CI between wells prior to treatment. The results are averages of duplicate treatments and the graphs are representative of findings obtained for at least 4 independent experiments.

The impedance data of the RT-CES™ analyser, which is a label free method for monitoring cell viability, cytotoxicity, adhesion and proliferation profiles of adherent cells, was successfully used in monitoring the differentiation of the THP-1 cells. THP-1 differentiation was first monitored for 48 h (with PMA) and 24 h (PMA free). During the 72 h period, sustained increases in CI were observed as the undifferentiated monocytes became differentiated into adherent macrophages (Figure 12). This was followed by treatment with the polymers and NPs for a further 72 h. Untreated cells maintained a relatively steady state with respect to CI changes for up to 30 h followed by a gradual decline in CI likely resulting from loss in cell integrity. The steady state maintained by the cells is supported by the fact that differentiated cells do not proliferate [32].

PLGA and C-PLGA polymer treated cells resulted in dose response profiles (Figure 12 A and B) not seen in the MTT study. The profile for C-PLGA was more profound with an initial increase in CI followed by a gradual drop to values as low as zero (at 40 and 100 µg/mL) which could be interpreted as cytotoxicity [16]. Peaks in the CI, attributed to uptake and cell swelling were observed for the polymers. Minimal uptake of PLGA was observed compared to C-PLGA (CI peaked at 1.9 ± 0.2 for C-PLGA compared to 1.1 ± 0.4 for PLGA at 40 µg/mL). At 100 µg/mL, no peak was observed for PLGA, and for C-PLGA the peak was diminished compared to that at 40 µg/mL attributable to a dose response loss of cell adhesion. Interestingly, microscopic examination revealed pronounced cell proliferation and clumping or aggregation in the C-PLGA treated cells (Figure 13), which we attributed to the immuno-stimulatory nature of the polymer. Cell stimulation causes morphological changes which result in changes in cellular impedance [33]. Surprisingly, MTT assay of the cells from the E-plate indicated cell viability (up to 100 % or more) of the cells treated with C-PLGA, likely due to stimulation (Figure 13 F). Considering that MTT and RT-CES data have previously been correlated, this finding was unexpected and points to the need to correlate data from different methods before conclusions are derived. These findings are crucial for studies involving testing of small molecules on differentiating cells in which impedance measurements or MTT assay are used as a tool for determining viability or cytotoxicity.

The profiles obtained for PLGA NPs and C-PLGA NPs (Figure 12 C and D) were similar to those of C-PLGA polymer in the first 3 h post treatment but with a reversal in the dose responsiveness. We attribute the reversal in dose responsiveness when compared to the
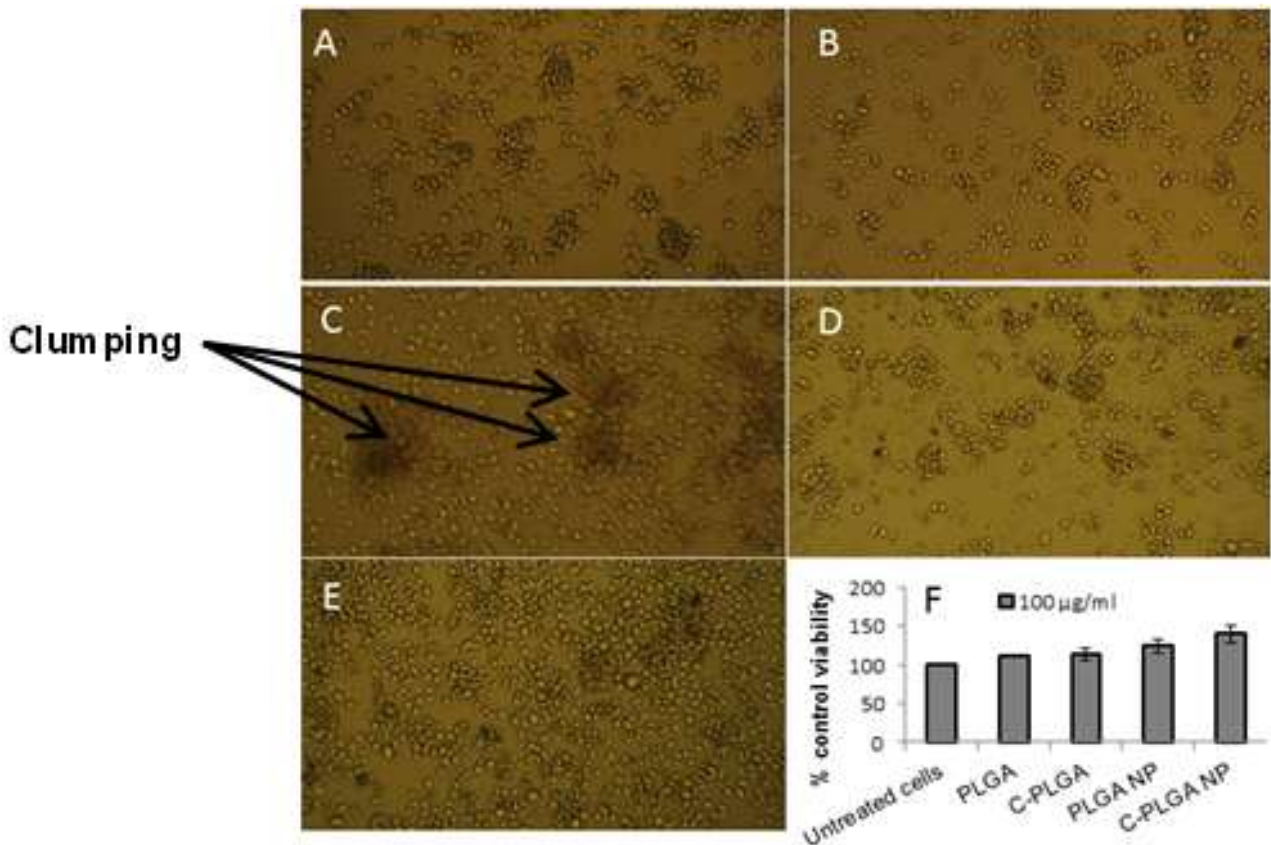
Figure 13: Phase images of cells treated with 100 µg/mL of polymers and NPs at 72 h post treatment. Images were obtained with an inverted microscope. Untreated cells are represented in A, PLGA treated cells in B, C-PLGA in C, PLGA NPs in D and C-PLGA NPs treated cells in E. The characteristic morphology of stimulated and proliferating cells (clumping and aggregations) is depicted for C-PLGA treated cells (C). This morphology is absent for cells in B, D and E. The C-PLGA (C) treated cells also appear more rounded (hence less adhesion) compared to cells treated with PLGA, PLGA NPs or C-PLGA NPs. The number of cells in E appears >D>C>B. Corresponding MTT treated cells are shown in F (n=2). According to the MTT data, C-PLGA NP treated cells were more viable than cells treated with PLGA, C-PLGA or PLGA NP. The viability data also appears to correspond with cell number as seen in images B-E i.e. E>D>C>B. All treated cells were more viable than untreated cells (>100 %) likely a result of the stimulatory nature of the treatments.

polymers, to the latter's effects on cell adhesion being dose dependent. Microscopically, PLGA NPs and C-PLGA NPs (Figure 13D and E) did not present the clumping observed for C-PLGA (Figure 13C) further supporting the differences in adhesion profiles. An initial short term increase in CI post treatment was observed which peaked at 1.5 ± 0.1 and 1.7 ± 0.1 following treatment with PLGA NPs and C-PLGA NPs respectively (100 µg/mL), compared to untreated cells (1.2 ± 0.1). Again this peaking was associated with uptake and swelling [14]. This was followed by a period in which CI dropped to below control levels (~ 0.7) within 8 h possibly due to changes in the cell morphology and hence decrease in adhesion. The

drop in CI for the NPs, unlike for C-PLGA polymer, was followed by gradual sustained increases in CI to form characteristic "spoon-shaped" profiles between 80 and 120 h. Such 'spoon shaped' profiles are associated with intracellular Ca^{2+} increases [34]. To determine any differences in Ca^{2+} signaling between the PLGA NPs and C-PLGA NPs, the negative area under the curve (for the "spoon shaped" structure) was calculated with 1 as baseline at 100 µg/mL using Graphpad Prism® (San Diego, California, USA). The area was found to be 20.7 ± 1.5 and 22.8 ± 5.6 for PLGA NPs and C-PLGA NPs respectively, (area for untreated cells was 13.6 ± 4.9), and no significant difference was observed between treatments (p > 0.05). Phagocytosis is a Ca^{2+} dependent process [35] and could explain the observation of 'spoon shaped' profiles for both NPs. Dose-dependency of the spoon shaped profiles was observed (0.4-100 µg/mL) suggesting increased phagocytosis. Interestingly, curdlan through Dectin-1 activation is known to increase intracellular Ca^{2+} following phosphorylation of various intracellular phospholipases [36], However, no significant difference in the areas of the spoon shaped profiles was observed between the C-PLGA NPs and PLGA NPs treated cells, possibly due to masking by phagocytosis.

Although the impedance data did not correlate with the MTT findings especially for C-PLGA (since adhesion receptors were altered), it was useful in providing valuable insights on the effects of the NPs on the macrophages with respect to Ca^{2+} modulation.. Additional studies to determine how adhesion of the treated cells was affected by determining the presence of adhesion receptors such as CD11c and CD18 which are predominantly expressed on differentiated THP-1 macrophages [37, 38] will be useful in understanding how polymers, in particular C-PLGA affect cell adhesion. These results are the first to the best of our knowledge to show Ca^{2+} signaling related uptake of NPs using impedance measurements.

Conclusion

We have shown successful synthesis of a bio-intergrated C-PLGA copolymer. NPs synthesized from this polymer possess immune-stimulatory activity, as well as sustained drug delivery potential. The polymers and NPs were non-toxic against THP-1 macrophages as determined by MTT assays. Real time impedance measurements of the macrophages in the presence of the polymers and NPs provided novel insights into uptake, adhesion profiles and stimulation, which were otherwise not discernible from the endpoint MTT assay. Dose dependent loss of macrophage adhesion was observed in the presence of the polymers, in particular C-PLGA. No loss of cell adhesion was observed in the case of NP treated cells. For the first time, the Ca^{2+} dependent uptake of NPs into macrophages has been demonstrated using impedance measurements and this could lead to increased application of this technology in studies involving NPs. We expect our results to lead to further development of bio-intergrated polymers and immunostimulatory NPs for cellular targeted therapy.

References

1. Lin, K. and A.M. Kasko, *Carbohydrate-Based Polymers for Immune Modulation.* ACS Macro Letters, 2014. **3**(7): p. 652-657.
2. Eggermont, A.M.M. and C. Robert, *Melanoma: Smart therapeutic strategies in immuno-oncology.* Nat Rev Clin Oncol, 2014. **11**(4): p. 181-182.

3. Dube, A., et al., *State of the art and future directions in nanomedicine for tuberculosis.* Expert Opinion on Drug Delivery, 2013. **10**(12): p. 1725-1734.

4. Dube, A., et al., *Multimodal nanoparticles that provide immunomodulation and intracellular drug delivery for infectious diseases.* Nanomedicine: Nanotechnology, Biology and Medicine, 2014. **10**(4): p. 831-838.

5. Ali, O.A., et al., *Infection-mimicking materials to program dendritic cells in situ.* Nat Mater, 2009. **8**(2): p. 151-158.

6. Lehtovaara, B.C., M.S. Verma, and F.X. Gu, *Synthesis of curdlan-graft-poly(ethylene glycol) and formulation of doxorubicin-loaded core–shell nanoparticles.* Journal of Bioactive and Compatible Polymers, 2012. **27**(1): p. 3-17.

7. Goodridge, H.S., A.J. Wolf, and D.M. Underhill, *β-glucan recognition by the innate immune system.* Immunological Reviews, 2009. **230**(1): p. 38-50.

8. Brown, G.D., et al., *Dectin-1 Is A Major β-Glucan Receptor On Macrophages.* The Journal of Experimental Medicine, 2002. **196**(3): p. 407-412.

9. Lei, L., et al., *Self-assembled nanoparticles of cholesterol-conjugated carboxymethyl curdlan as a novel carrier of epirubicin.* Nanotechnology, 2010. **21**(26): p. 265601.

10. Vashist, S.K., *Comparison of 1-Ethyl-3-(3-Dimethylaminopropyl) Carbodiimide Based Strategies to Crosslink Antibodies on Amine-Functionalized Platforms for Immunodiagnostic Applications.* Diagnostics, 2012. **2**(3): p. 23-33.

11. Hayeshi, R., et al., *Comparison of drug transporter gene expression and functionality in Caco-2 cells from 10 different laboratories.* European Journal of Pharmaceutical Sciences, 2008. **35**(5): p. 383-396.

12. Alley, M.C., et al., *Feasibility of Drug Screening with Panels of Human Tumor Cell Lines Using a Microculture Tetrazolium Assay.* Cancer Research, 1988. **48**(3): p. 589-601.

13. Fonteh, P.N., F.K. Keter, and D. Meyer, *New bis(thiosemicarbazonate) gold(III) complexes inhibit HIV replication at cytostatic concentrations: Potential for incorporation into virostatic cocktails.* Journal of Inorganic Biochemistry, 2011. **105**(9): p. 1173-1180.

14. Thakur, M., et al., *Real time monitoring of the cell viability during treatment with tumor-targeted toxins and saponins using impedance measurement.* Biosensors and Bioelectronics, 2012. **35**(1): p. 503-506.

15. Atienza, J.M., et al., *Dynamic Monitoring of Cell Adhesion and Spreading on Microelectronic Sensor Arrays.* Journal of Biomolecular Screening, 2005. **10**(8): p. 795-805.

16. Xing, J.Z., et al., *Microelectronic cell sensor assay for detection of cytotoxicity and prediction of acute toxicity.* Toxicology in Vitro, 2006. **20**(6): p. 995-1004.

17. Solly, K., et al., *Application of real-time cell electronic sensing (RT-CES) technology to cell-based assays.* Assay Drug Dev Technol, 2004. **2**(4): p. 363-72.

18. Fukuhara, G. and Y. Inoue, *Oligosaccharide sensing with chromophore-modified curdlan in aqueous media.* Chemical Communications, 2010. **46**(48): p. 9128-9130.

19. Wei, K., X. Peng, and F. Zou, *Folate-decorated PEG–PLGA nanoparticles with silica shells for capecitabine controlled and targeted delivery.* International Journal of Pharmaceutics, 2014. **464**(1–2): p. 225-233.

20. Bothara, S.B. and S. Singh, *Thermal studies on natural polysaccharide.* Asian Pacific Journal of Tropical Biomedicine, 2012. **2**(2, Supplement): p. S1031-S1035.

21. Khayet, M., M.M. Nasef, and J.I. Mengual, *Radiation grafted poly(ethylene terephthalate)-graft-polystyrene pervaporation membranes for organic/organic separation.* Journal of Membrane Science, 2005. **263**(1–2): p. 77-95.

22. Shi, L., *Characterization of the flame retardancy of EVA copolymer by plasma grafting of acrylic acid.* European Polymer Journal, 2000. **36**(12): p. 2611-2615.

23. Athawale, V.D. and V. Lele, *Syntheses and characterisation of graft copolymers of maize starch and methacrylonitrile.* Carbohydrate Polymers, 2000. **41**(4): p. 407-416.

24. Yu, L., et al., *Synthesis and characterization of novel biodegradable folate conjugated polyurethanes.* Journal of Colloid and Interface Science, 2011. **358**(2): p. 376-383.

25. Suchao-in, K., P. Koombhongse, and S. Chirachanchai, *Starch grafted poly(butylene succinate) via conjugating reaction and its role on enhancing the compatibility.* Carbohydrate Polymers, 2014. **102**(0): p. 95-102.

26. Ping, X., M. Wang, and X. Ge, *Radiation induced graft copolymerization of n-butyl acrylate onto poly(ethylene terephthalate) (PET) films and thermal properties of the obtained graft copolymer.* Radiation Physics and Chemistry, 2011. **80**(5): p. 632-637.

27. Chimamkpam, E.F.C., et al., *Dynamic Stability of Organic Conducting Polymers and Its Replication in Electrical Conduction and Degradation Mechanisms.* Advanced Functional Materials, 2011. **21**(12): p. 2240-2250.

28. Sahana, D.K., et al., *PLGA nanoparticles for oral delivery of hydrophobic drugs: Influence of organic solvent on nanoparticle formation and release behavior In Vitro and In Vivo using estradiol as a model drug.* Journal of Pharmaceutical Sciences, 2008. **97**(4): p. 1530-1542.

29. Plato, A., J.A. Willment, and G.D. Brown, *C-type lectin-like receptors of the dectin-1 cluster: ligands and signaling pathways.* Int Rev Immunol, 2013. **32**(2): p. 134-56.

30. Schluger, N., W. and W. Rom, N., *The Host Immune Response to Tuberculosis.* American Journal of Respiratory and Critical Care Medicine, 1998. **157**(3): p. 679-691.

31. Gostner, J.M., et al., *Redox regulation of the immune response.* Redox Rep, 2013. **18**(3): p. 88-94.

32. Schwende, H., et al., *Differences in the state of differentiation of THP-1 cells induced by phorbol ester and 1,25-dihydroxyvitamin D3.* Journal of Leukocyte Biology, 1996. **59**(4): p. 555-61.

33. Denelavas, A., et al., *Real-time cellular impedance measurements detect Ca(2+) channel-dependent oscillations of morphology in human H295R adrenoma cells.* Biochim Biophys Acta, 2011. **1813**(5): p. 754-62.

34. Abassi, Y.A., et al., *Dynamic monitoring of beating periodicity of stem cell-derived cardiomyocytes as a predictive tool for preclinical safety assessment.* British Journal of Pharmacology, 2012. **165**(5): p. 1424-1441.

35. Nunes, P. and N. Demaurex, *The role of calcium signaling in phagocytosis.* J Leukoc Biol, 2010. **88**(1): p. 57-68.

36. Xu, S., et al., *Phospholipase Cγ2 Is Critical for Dectin-1-mediated Ca2+ Flux and Cytokine Production in Dendritic Cells.* Journal of Biological Chemistry, 2009. **284**(11): p. 7038-7046.

37. Spano, A., et al., *Expression of cell kinetics and death during monocyte–macrophage differentiation: effects of Actinomycin D and Vinblastine treatments.* Histochemistry and Cell Biology, 2007. **127**(1): p. 79-94.

38. Plescia, J. and D.C. Altieri, *Activation of Mac-1 (CD11b/CD18)-bound factor X by released cathepsin G defines an alternative pathway of leucocyte initiation of coagulation.* Biochem J, 1996. **319 (Pt 3)**: p. 873-9.